

3D magnetic-field morphology of the Perseus molecular cloud

M. Tahani, W. Lupypciw, J. Glover, R. Plume, J. L. West, R. Kothes, S. Inutsuka, M. -Y. Lee, T. Robishaw, L. B. G. Knee, et al.

▶ **To cite this version:**

M. Tahani, W. Lupypciw, J. Glover, R. Plume, J. L. West, et al.. 3D magnetic-field morphology of the Perseus molecular cloud. Astronomy and Astrophysics - A&A, 2022, 660, 10.1051/0004-6361/202141170 . insu-03745333

HAL Id: insu-03745333
https://insu.hal.science/insu-03745333

Submitted on 4 Aug 2022

HAL is a multi-disciplinary open access archive for the deposit and dissemination of scientific research documents, whether they are published or not. The documents may come from teaching and research institutions in France or abroad, or from public or private research centers.

L'archive ouverte pluridisciplinaire **HAL**, est destinée au dépôt et à la diffusion de documents scientifiques de niveau recherche, publiés ou non, émanant des établissements d'enseignement et de recherche français ou étrangers, des laboratoires publics ou privés.

A&A 660, A97 (2022)
https://doi.org/10.1051/0004-6361/202141170
© ESO 2022

Astronomy & Astrophysics

3D magnetic-field morphology of the Perseus molecular cloud

M. Tahani[1], W. Lupypciw[1,2], J. Glover[1,3], R. Plume[2], J. L. West[4], R. Kothes[1], S. Inutsuka[5], M.-Y. Lee[6], T. Robishaw[1], L. B. G. Knee[7], J. C. Brown[2], Y. Doi[8], I. A. Grenier[9], and M. Haverkorn[10]

[1] Dominion Radio Astrophysical Observatory, Herzberg Astronomy and Astrophysics Research Centre, National Research Council Canada, PO Box 248, Penticton, BC V2A 6J9, Canada
e-mail: mtahani@ucalgary.ca
[2] Department of Physics & Astronomy, University of Calgary, Calgary, Alberta T2N 1N4, Canada
[3] Department of Physics & Astronomy, University of Victoria, Victoria, British Columbia V8P 5C2, Canada
[4] Dunlap Institute for Astronomy and Astrophysics University of Toronto, Toronto, ON M5S 3H4, Canada
[5] Department of Physics, Graduate School of Science, Nagoya University, Furo-cho, Chikusa-ku, Nagoya 464-8602, Japan
[6] Korea Astronomy and Space Science Institute, 776 Daedeok-daero, 34055 Daejeon, Republic of Korea
[7] Herzberg Astronomy and Astrophysics Research Centre, National Research Council Canada, 5071 West Saanich Road, Victoria BC V9E 2E7, Canada
[8] Department of Earth Science and Astronomy, Graduate School of Arts and Sciences, The University of Tokyo, 3-8-1 Komaba, Meguro, Tokyo 153-8902, Japan
[9] Université de Paris and Université Paris Saclay, CEA, CNRS, AIM, 91190 Gif-sur-Yvette, France
[10] Department of Astrophysics/IMAPP, Radboud University, PO Box 9010, 6500 GL Nijmegen, The Netherlands

Received 23 April 2021 / Accepted 16 February 2022

ABSTRACT

Context. Despite recent observational and theoretical advances in mapping the magnetic fields associated with molecular clouds, their three-dimensional (3D) morphology remains unresolved. Multi-wavelength and multi-scale observations will allow us to paint a comprehensive picture of the magnetic fields of these star-forming regions.
Aims. We reconstructed the 3D magnetic field morphology associated with the Perseus molecular cloud and compared it with predictions of cloud-formation models. These cloud-formation models predict a bending of magnetic fields associated with filamentary molecular clouds. We compared the orientation and direction of this field bending with our 3D magnetic-field view of the Perseus cloud.
Methods. We used previous line-of-sight and plane-of-sky magnetic field observations as well as Galactic magnetic field models to reconstruct the complete 3D magnetic field vectors and morphology associated with the Perseus cloud.
Results. We approximated the 3D magnetic field morphology of the cloud as a concave arc that points in the decreasing longitude direction in the plane of the sky (from our point of view). This field morphology preserves a memory of the Galactic magnetic field. In order to compare this morphology to cloud-formation model predictions, we assume that the cloud retains a memory of its most recent interaction. After incorporating velocity observations, we find that the line-of-sight magnetic field observations are consistent with predictions of shock-cloud-interaction models.
Conclusions. To our knowledge, this is the first time that the 3D magnetic fields of a molecular cloud have been reconstructed. We find the 3D magnetic field morphology of the Perseus cloud to be consistent with the predictions of the shock-cloud-interaction model that describes the formation mechanism of filamentary molecular clouds.

Key words. stars: formation – ISM: magnetic fields – ISM: clouds – evolution – magnetic fields – ISM: general

1. Introduction

Molecular clouds in which stars form are often shaped as elongated filamentary structures or filaments (e.g., Molinari et al. 2010; André et al. 2010, 2014; Arzoumanian et al. 2011). Within these structures, magnetic fields play an important role in the star-formation process (e.g., McKee & Ostriker 2007; Hennebelle & Falgarone 2012; Seifried & Walch 2015; Hennebelle & Inutsuka 2019; Pudritz & Ray 2019; Pattle & Fissel 2019). Determining the three-dimensional (3D) magnetic field morphology (Houde et al. 2004; Li & Houde 2008) of these star-forming regions will enable us to characterize their role in the process. Recent studies (e.g., Chen et al. 2019; Tahani et al. 2019; Hu et al. 2020) have investigated these 3D fields using a range of techniques.

To fully probe 3D magnetic fields, observations of both the plane-of-sky and the line-of-sight components of magnetic fields ($B_\perp$ and $B_\parallel$, respectively) are necessary. Recent observations have made significant progress in mapping the $B_\perp$ of molecular clouds (e.g., Planck Collaboration Int. XXXV 2016; Fissel et al. 2016; Pattle et al. 2019; Doi et al. 2020). Planck Collaboration Int. XXXII (2016); Planck Collaboration Int. XXXV (2016) showed that $B_\perp$ lines tend to be perpendicular to high column density ($>10^{21.7}$ cm^{-2}) filamentary structures and parallel to lower column density ones. Simulations show that magnetic fields perpendicular to the filaments allow for greater mass accumulations and result in denser filaments (e.g., Inoue et al. 2018; Hennebelle & Inutsuka 2019).

A recent study by Tahani et al. (2018) developed a new technique based on Faraday rotation measurements to map the $B_\parallel$ associated with molecular clouds[1]. They found that in some

[1] Recently updated code for determining $B_\parallel$ is available at https://github.com/MehrnooshTahani/MappingBLOS_MolecularClouds

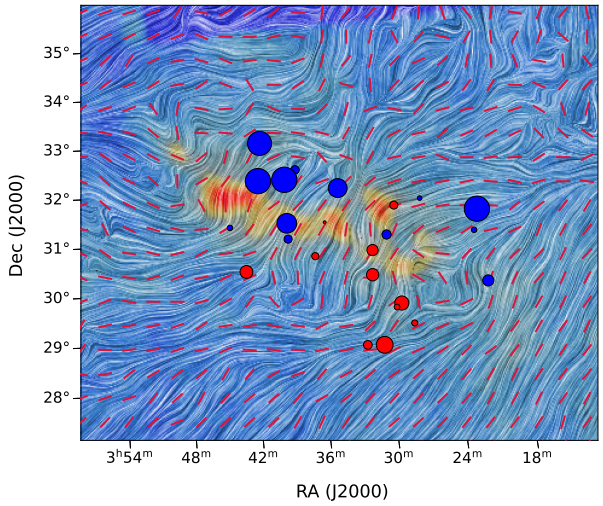


Fig. 1. Observed magnetic fields in the vicinity of the Perseus molecular cloud. The $B_\perp$ lines were observed by the *Planck* Space Observatory and the $B_\parallel$ were obtained by Tahani et al. (2018). The red and drapery lines show the $B_\perp$, and the blue (red) circles show magnetic fields toward (away from) us. The size of the circles represents the strength of the magnetic fields. The background color image is the visual extinction map obtained by Kainulainen et al. (2009).

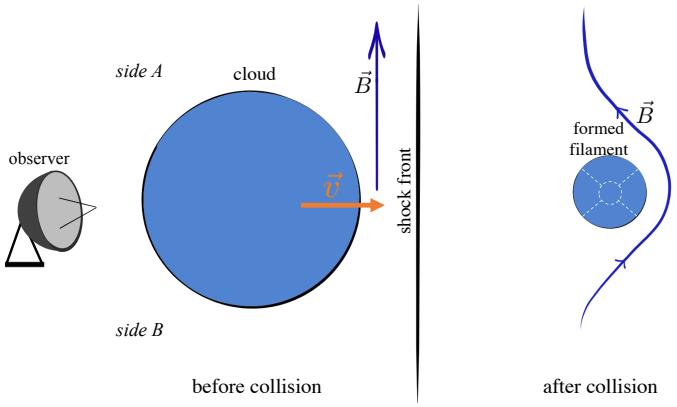


Fig. 2. Formation of an arc-shaped magnetic field morphology around filamentary molecular clouds as described by Inoue et al. (2018). After the interaction between the cloud and shock-front, with the velocity $\boldsymbol{v}$ in the co-moving frame of the shock-front, a filamentary structure is formed (shown in an end-on view in the right side); $\boldsymbol{B}$ shows the direction of the initial magnetic field before the collision and the morphology of the magnetic field after the collision. The resulting field structure in this image is concave from the observer's vantage point.

molecular clouds, including the Perseus cloud, the $B_\parallel$ direction reverses from one side of these filamentary clouds to the other side (perpendicular to the cloud's long axis), as shown in Fig. 1. In this figure, the background color image shows the visual extinction map (in units of magnitude of visual extinction or A_V) of the Perseus cloud provided by Kainulainen et al. (2009), where they obtained near-infrared dust extinction maps using the 2MASS data archive and the NICEST (Lombardi 2009) color excess mapping technique. The blue (red) circles show magnetic fields toward (away from) us. The red and drapery lines (made using the line integration convolution technique[2], Cabral & Leedom 1993) show the $B_\perp$ observed by *Planck*. In addition, Planck Collaboration Int. XXXV (2016) and Soler (2019) showed that $B_\perp$ is mostly perpendicular to the Perseus cloud.

An arc-shaped[3] magnetic field morphology has been proposed to explain this $B_\parallel$ reversal across the clouds. For example, Heiles (1997) suggested that an arc-shaped magnetic field morphology should be present associated with the Orion A cloud, due to recurrent shocks by nearby supernovae in the Orion-Eridanus bubble. Tahani et al. (2019) showed that an arc-shaped magnetic field morphology was the most likely candidate among the magnetic morphologies that could explain a $B_\parallel$ reversal across the Orion A filamentary cloud.

Moreover, studies of Doi et al. (2021) and Bialy et al. (2021) have suggested that bubbles in the Perseus-Taurus region have formed the Perseus molecular cloud. Formation of clouds through expanding bubbles can result in an arc-shaped magnetic field morphology associated with the filamentary structures (Inoue & Fukui 2013; Inutsuka et al. 2015; Inoue et al. 2018; Abe et al. 2021). These cloud-formation studies suggest that dense filamentary molecular clouds form via interaction of a shock front and a pre-existing inhomogeneous dense cloud, where the magnetic fields are predicted to bend and allow for further mass accumulation, creating even denser filaments. This results in filaments or filamentary structures with an arc-shaped magnetic field around them. In this scenario (shock-cloud interaction; hereafter SCI model), the interaction occurs between a relatively dense cloud ($\sim 10^3$ cm^{-3}) and a shock wave propagating in low density gas (HI), as illustrated in Fig. 2.

In general, the shock wave propagation direction is not aligned with the mean magnetic field. Therefore, the SCI model considers a perpendicular magnetic field ($\boldsymbol{B} \perp \boldsymbol{v}$) as illustrated in Fig. 2. This process is studied in detail by Abe et al. (2021) as a formation mechanism of filamentary structures on smaller scales (of a few pc). However, the resultant geometry of the shock-cloud interaction is scale-free and should be the same on larger scales. Evidence of magnetic field bending due to environmental effects has been observed on large scales (~100 pc; Soler et al. 2018; Bracco et al. 2020).

In this study, we investigate the 3D magnetic field morphology of the Perseus molecular cloud, which is actively forming a significant number of low- to intermediate-mass stars (Bally et al. 2008). This cloud encompasses 10^4 solar masses ($M_\odot$; Bally et al. 2008) and has a distance of 294 ± 10 pc from the Sun (Zucker et al. 2019). The formation scenario proposed in the studies of Doi et al. (2020) and Bialy et al. (2021) indicates a high likelihood for an arc-shaped magnetic field morphology in this region.

We explore the direction and the shape of this arc-shaped field morphology in this study and reconstruct the most likely 3D magnetic field morphology associated with the Perseus cloud. For this purpose, we incorporated the $B_\parallel$ and $B_\perp$ observations of Tahani et al. (2018) and Planck Collaboration Int. XXXV (2016), as well as Galactic magnetic field (GMF) models to estimate the initial magnetic field orientation and direction in this region. We then compare this 3D magnetic field morphology with cloud-formation model predictions. To this end, we used the HI and CO velocity observations in this region, as well as other studies and observational data indicating interactions between the Perseus cloud and its surroundings.

Section 2 presents the observational data that are used in this study. We discuss our approach and reconstruct the Perseus cloud's 3D magnetic field in Sect. 3. We compare the obtained

[2] https://pypi.org/project/licpy/

[3] Previously called bow-shaped (Tahani et al. 2019); pronounced /bō/ as in rainbow or bow and arrow.

3D magnetic field with the predictions of cloud-formation models in Sect. 4, using velocity observations. Finally, we provide a general discussion in Sect. 5, followed by a summary and conclusion in Sect. 6.

2. Data used in the study

We incorporate estimates of the initial 3D magnetic field direction, cloud velocities, and the present-state $B_\parallel$ observations associated with the Perseus cloud. To estimate the initial magnetic field direction, we use magnetic field models of the Galaxy. To determine the cloud velocities, we use available CO and HI observations. For the $B_\parallel$, we use the catalog of Tahani et al. (2018). We expand on these data below.

2.1. Galactic magnetic field

We use the Jansson & Farrar (2012, hereafter referred to as JF12) Galactic magnetic field model to estimate the direction of the initial magnetic fields. The JF12 model contains a two-dimensional (2D) thin-disk field component closely associated with the Galactic spiral arms, an azimuthal-toroidal halo field component, and an X-shaped vertical-and-out-of-plane field component. In addition to the regular field, the JF12 model includes an optional striated random field component. Jansson & Farrar (2012) constrained their random model parameters based on Faraday rotation measurements and polarized synchrotron radiation from the Wilkinson Microwave Anisotropy Probe (WMAP) seven-year release (WMAP7) synchrotron emission data.

To estimate the GMF in the vicinity of the Perseus molecular cloud, we used the Hammurabi program (Waelkens et al. 2009). The Hammurabi program[4] is a synchrotron modeling code that has been used in several works (e.g., Planck Collaboration Int. XLII 2016; Jansson & Farrar 2012) to produce simulated maps, which are then compared to data and used to constrain the model. These models are included with the code, and we can use the Hammurabi code to estimate the GMF vectors in Cartesian coordinates at a particular location in the Galaxy corresponding to the position of the molecular cloud.

2.2. Velocity information

We considered both the available CO and HI velocities. The CO and HI observations enable us to explore the line-of-sight velocities of the molecular and the atomic regions, respectively. We discuss these velocity data in this subsection.

HI data. For the HI velocity information, we used the all-sky HI database of the HI 4π Survey (HI4PI; HI4PI Collaboration 2016) with an angular resolution of 16.2′. HI4PI is based on the Effelsberg-Bonn HI Survey (EBHIS; Kerp et al. 2011; Winkel et al. 2016), using the Effelsberg 100-m telescope, and the Galactic All-Sky Survey (GASS; McClure-Griffiths et al. 2009) made with the Parkes 64-m telescope. The HI4PI survey has a spectral resolution of 1.49 km s^{-1}, channel separation of 1.29 km s^{-1}, and velocity range of $|v_{\rm LSR}| \leq 600$ km s^{-1} for the northern (EBHIS) and $|v_{\rm LSR}| \leq 400$ km s^{-1} for the southern (GASS) parts in the Local Standard of Rest frame (LSR). The significant overlap between EBHIS and GASS ($-5^\circ \leq \delta \leq 0.5^\circ$) allowed for the accurate merging of the two surveys in creating the HI4PI survey.

CO data. To approximate the motion of each cloud, we used the radial velocities from the Dame et al. (2001) carbon monoxide survey. This catalog is a survey of the ^{12}CO J(1–0) spectral line of the Galaxy at 115 GHz with the pixel spacing of 7.5′ and velocity resolution of 1.3 km s^{-1} (obtained with the CfA 1.2-m telescope and a similar telescope on Cerro Tololo in Chile).

2.3. Line-of-sight magnetic field

We use the $B_\parallel$ catalog of Tahani et al. (2018). They used Faraday rotation measurements to determine $B_\parallel$ in and around four filamentary molecular clouds. To find $B_\parallel$, these authors used a simple approach based on relative measurements to estimate the amount of rotation measure induced by the molecular clouds versus that induced by the rest of the Galaxy. They then determined $B_\parallel$ using the rotation measure catalog of Taylor et al. (2009), a chemical evolution code, and the Kainulainen et al. (2009) extinction maps (for more details, see Tahani et al. 2018). They found that the $B_\parallel$ direction in the Perseus molecular cloud reverses from one side of the cloud to the other, as shown in Fig. 1.

3. Main results: reconstructing the 3D magnetic field morphology of the Perseus cloud

Recent studies (Doi et al. 2021; Bialy et al. 2021) suggest that the Perseus molecular cloud formed as the result of interaction with bubbles (i.e., the SCI model). Bialy et al. (2021) proposed that multiple supernovae created a bubble resulting in formation of the Perseus molecular cloud. The presence of bubbles and their contribution to the formation and evolution of the Perseus cloud, along with the observed $B_\parallel$ reversal, as shown in Fig. 1, suggest a model for the arc-shaped magnetic field morphology based on shock interaction in this region. Using the initial magnetic field vectors in this region and the orientation of $B_\parallel$ reversal, we can reconstruct the complete 3D morphology of the arc-shaped magnetic field associated with the Perseus cloud.

3.1. Galactic magnetic field in the region

To determine the initial magnetic field direction, we used a GMF model based on JF12. This GMF model does not include the isotropic random field component, that is, small-scale Gaussian random field (Jaffe et al. 2010), which arises from the zeroth-order simplification of the ISM turbulence and other environmental elements (Haverkorn 2015; Jaffe 2019, see their Fig. 1). We refer to this structure as the "coherent GMF" model. To best describe the GMF vectors and compare them with the $B_\parallel$ and $B_\perp$ observations, we used a frame of reference as shown in Fig. 3, where the $\hat{\ell}$, $\hat{b}$, and $\hat{d}$ axes point in the increasing longitude, latitude, and distance directions (of the Perseus cloud's approximate center location), respectively.

We delineate a volume around the Perseus molecular cloud to model the GMF, ∼200 pc deep along the line of sight (with ∼100 pc in front of and behind the 294 pc average cloud distance), spanning $\sim 11^\circ \times 11^\circ$ (104 pc^2) in the plane of the sky. We set a resolution of one GMF vector per 2 pc × 2 pc × 2 pc. Figure 4 illustrates the plane-of-sky GMF unit vectors (red arrows) at the location of the Perseus cloud for this coherent GMF model, overlaid on the extinction map of this cloud. These also match previous studies and their modeled GMF vectors at this location (e.g., Van Eck et al. 2011, see their Fig. 6). We find that the coherent GMF lies mostly perpendicular to the main axis of Perseus. We estimate the unit vector showing the direction of the coherent GMF in our frame of reference to be $-0.99\hat{\ell} + 0.15\hat{b} - 0.01\hat{d}$.

[4] http://sourceforge.net/projects/hammurabicode/

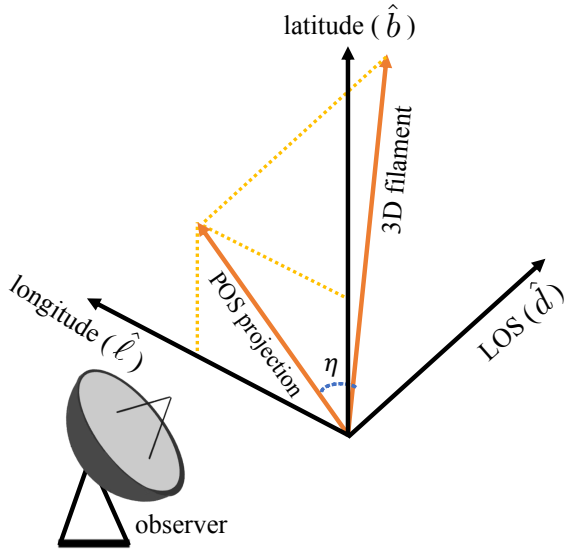


Fig. 3. Reference frame in our study. Longitude ($\hat{\ell}$) and latitude ($\hat{b}$) axes are pointing in the increasing direction of Galactic longitude and latitude (at the center location of the Perseus cloud in the plane of the sky), respectively. The line-of-sight ($\hat{d}$) axis points in the direction of increasing distance from us. The angle η is the inclination angle of the filament with respect to the plane of the sky.

3.2. Complete 3D magnetic field morphology of the Perseus cloud

Knowing a high likelihood for the presence of an arc-shaped magnetic field morphology in this region, we reconstruct the complete 3D magnetic field morphology of this cloud. For this purpose, we used the $B_{\parallel}$ observations and the coherent Galactic magnetic field in this region.

Ideal magnetohydrodynamic (MHD) simulations (e.g., Li & Klein 2019) show that strong enough magnetic fields (with Alfvén mach number $\mathcal{M}_{\rm A} \simeq 1$) retain a memory of the initial large-scale magnetic field lines. If the initial magnetic fields are weak ($\mathcal{M}_{\rm A} \simeq 10$), the magnetic fields will get completely distorted, without following any particular large-scale morphology.

Both the $B_{\parallel}$ (Tahani et al. 2018) and the $B_{\perp}$ (Planck Collaboration Int. XXXV 2016) observations show that the large-scale magnetic fields associated with the Perseus cloud are coherent, as illustrated in Fig. 1. The $B_{\perp}$ lines are mostly perpendicular to the cloud's axis and the $B_{\parallel}$ reverses direction from one side of the cloud's axis to the other. The $B_{\perp}$ orientation for the Perseus cloud, as studied by the histograms of relative orientation in Planck Collaboration Int. XXXV (2016) and Soler (2019), is mostly perpendicular to the cloud's axis (when projected onto the plane of the sky) and overall in the same orientation as our modeled coherent GMF lines. These large-scale coherent magnetic fields indicate that the initial field lines have become more ordered and stronger during the cloud's formation and evolution. In other words, these magnetic fields retained a memory of the initial field lines and have not become completely distorted. We discuss this in a more quantitative manner in Sect. 5.

The direction of the GMF component, as shown in Fig. 4, is mostly perpendicular to the Perseus cloud filament axis and pointing from southeast side of the cloud to northwest in the equatorial coordinate system. Since the cloud preserves a memory of the large-scale GMF, this GMF direction, along with the $B_{\parallel}$ directions, indicate that the arc-shaped field morphology must be concave from the observer's point of view, with its plane-of-sky component pointing in the $-\hat{\ell}$ direction. Figure 5 shows a cartoon diagram of the complete 3D morphology of the magnetic fields in the Perseus cloud[5].

This 3D magnetic field morphology results in magnetic field lines projected on the plane of the sky that are consistent with the *Planck* $B_{\perp}$ observations. We note that the distances along the Perseus cloud (Zucker et al. 2018, 2020, 2021) suggest a relatively small inclination angle for the Perseus cloud. While we consider the cloud to be nearly parallel to the plane of the sky, larger inclination angles have no significant effect on the reconstructed 3D magnetic field morphology.

4. Comparison of the result with cloud-formation model predictions

Doi et al. (2021, see their Figs. 10 and 11) identify a dust cavity in this region, where the Perseus and Taurus clouds are located on the far- and near-sides of its shell, respectively. Bialy et al. (2021, see their Fig. 2) provide 3D modeling of this bubble and refer to it as Per-Tau. Bialy et al. (2021) propose that this bubble has swept up the interstellar medium and has ultimately led to the formation of the Perseus and Taurus molecular clouds. We illustrate this bubble projected on the plane of the sky as a white dash-dotted circle in Fig. 6, and as a 3D gray sphere in Fig. 7.

Bialy et al. (2021) suggested that this shell has swept-up the interstellar medium and has ultimately led to the formation of the Perseus and Taurus molecular clouds. They also found that multiple supernovae have likely contributed to the formation of this shell and explained the formation of the Perseus cloud through the multi-compression SCI model of Inutsuka et al. (2015). In this scenario, an initial bubble expansion can accumulate the ISM on the shell of a bubble, creating a relatively dense cloud. Subsequently, recurrent compressions from other (or the same) bubbles can result in a dense filamentary molecular cloud.

Additionally, Pon et al. (2016) observed an excess emission of the CO J(6-5) transition in the Perseus molecular cloud, indicating the presence of low-velocity shocks (and their turbulence dissipation). Pon et al. (2014) found similar CO J(6-5) emission in Barnard 1 (B1; Bachiller & Cernicharo 1984) region within the Perseus cloud. The confirmed presence of shocks in the Perseus cloud provides additional evidence for the formation and evolution of the Perseus cloud, as predicted by the SCI model.

Using the SCI model, if we are able to estimate the initial magnetic field direction as well as the velocity of the dense cloud (CO) and its HI surroundings, we will be able to predict the $B_{\parallel}$ direction associated with the cloud and its 3D magnetic field morphology (as shown in Fig. 2). We can compare these predictions with the $B_{\parallel}$ observations of Tahani et al. (2018) and our reconstructed magnetic fields. To this end, we used the coherent GMF direction to estimate the initial magnetic field direction in the region, and we assume that the cloud retains a memory of the most recent shock, interaction, or compression. To properly define the velocities, we consider the average velocity of the pre-existing cloud, $\boldsymbol{v}$, in the co-moving frame of the mean shock front. In general, the velocity is not aligned with the mean magnetic field, so we can assume that the field lines have a perpendicular component to the propagation direction, as illustrated in Fig. 2.

[5] The .obj files are available at https://github.com/MehrnooshTahani/Perseus3DMagneticFields

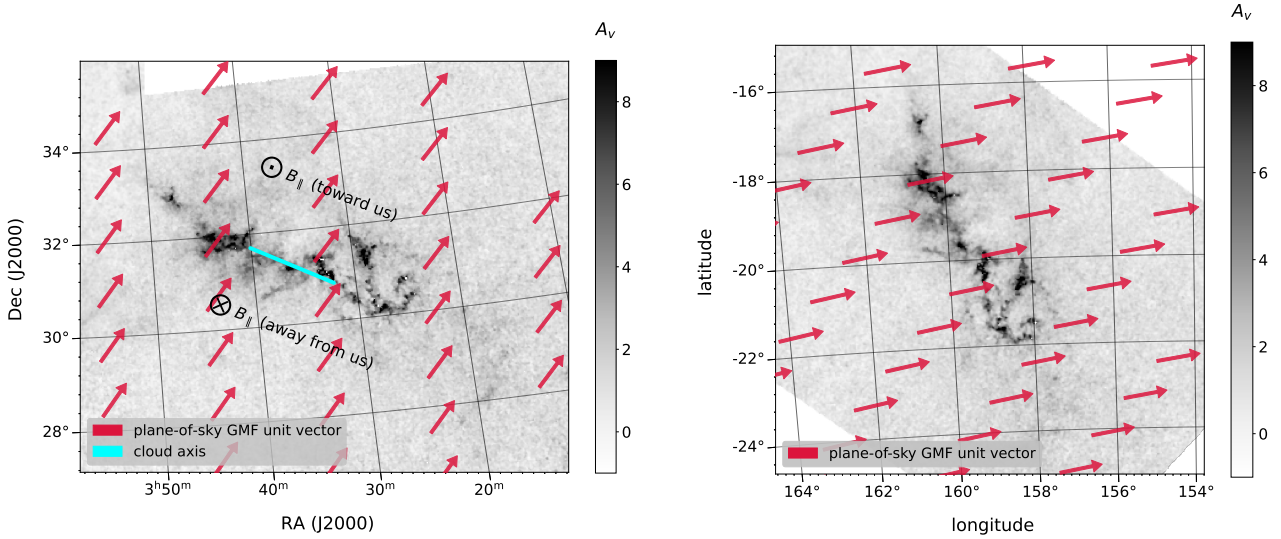


Fig. 4. Plane-of-sky GMF unit vectors over the Perseus molecular cloud showing the coherent GMF model obtained from the Hammurabi code. The background gray-scale image shows the extinction map from Kainulainen et al. (2009). The red vectors show the GMF unit vectors in the plane of the sky. *Left panel*: Cyan line represents the approximate filament axis, with $B_\parallel$ directions reversing in the direction perpendicular to this axis. *Right panel*: for the ease of comparison with Fig. 5, the Perseus cloud and GMF vectors are shown in galactic coordinates.

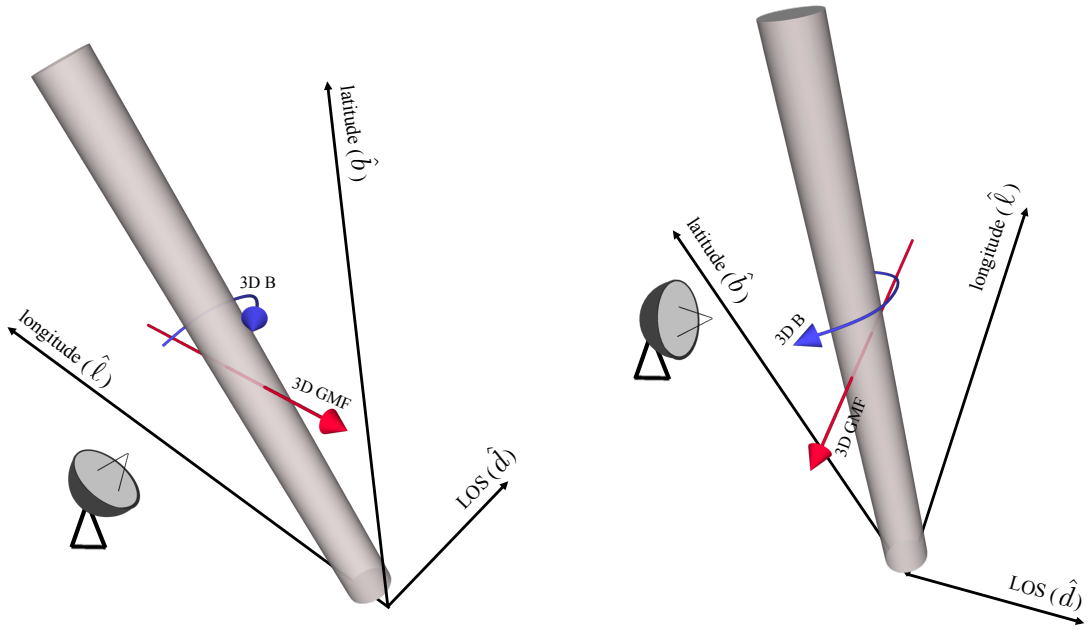


Fig. 5. 3D magnetic field morphology of the Perseus cloud. The gray cylinder, red vector, and blue arrow illustrate the filamentary cloud, the estimated Galactic magnetic field, and the reconstructed 3D magnetic field morphology associated with the cloud, respectively. The 3D magnetic field morphology is concave from the observer's point of view. The *left and right panels* show different viewing angles.

This interaction bends the magnetic field lines such that if $\boldsymbol{v}$ (velocity of the dense cloud in the HI co-moving frame) is pointing toward (away from) us, a convex (concave) bend in the field lines will be created from the observer's point of view. Additionally, the direction of this arc-shaped magnetic field, causing a $B_\parallel$ reversal, can be predicted. For example, if the initial magnetic field is pointing from side B to side A in Fig. 2, the concave pattern will result in magnetic field lines pointing toward the observer on side A and away from the observer on side B, resulting in a $B_\parallel$ reversal across the filament. To compare the magnetic field observations with the cloud-formation model predictions, we investigate the velocities of the cloud. In this comparison, we assume that while the velocities prior to the interaction (between the cloud and the shock front) have largely dissipated, the current-state direction of the cloud's velocity in the HI frame retains a memory of the most recent interaction.

4.1. Velocities

We first considered the galactic rotation velocities in this region to paint a comprehensive picture. On the scales of a giant molecular cloud and the Galaxy, we can assume that the conditions for ideal MHD hold true (Hennebelle & Inutsuka 2019) and the field lines are frozen in the interstellar medium (the filamentary structure and its surroundings). We used the model of Clemens (1985) with the IAU standard values of the solar distance from

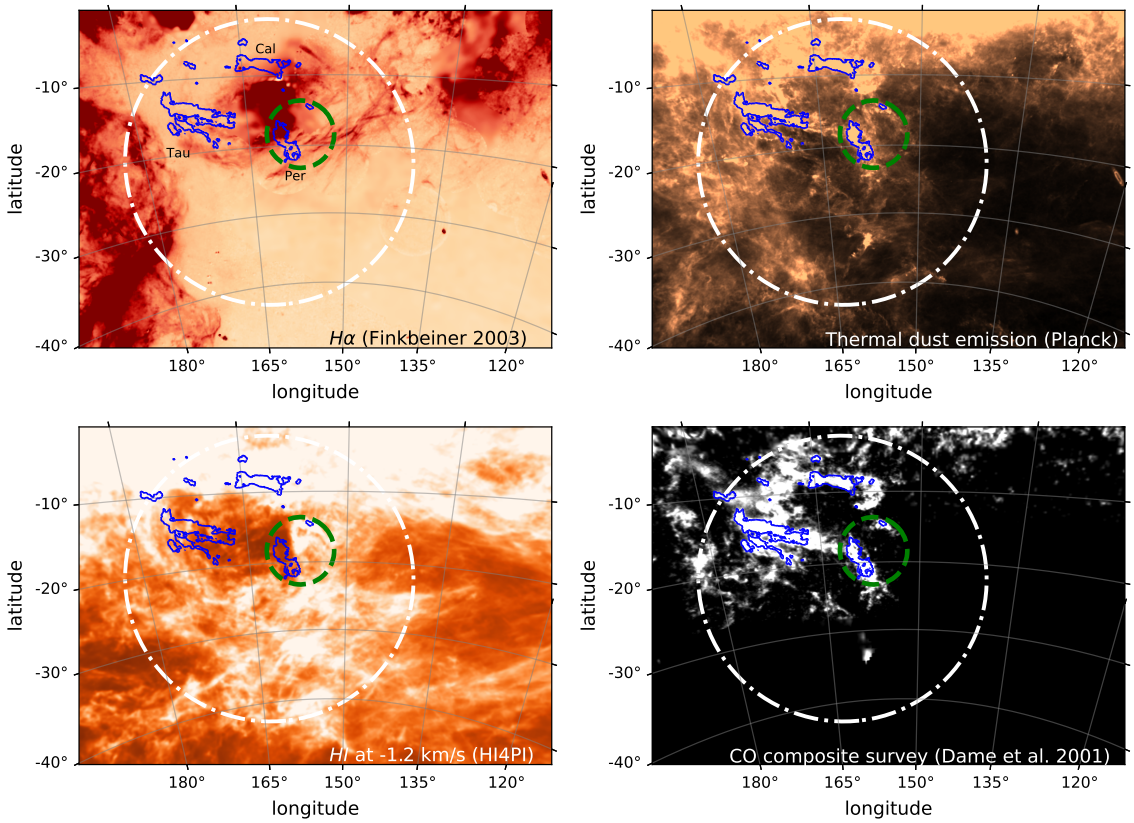


Fig. 6. Multi-wavelength observations of the Perseus cloud and associated bubbles. *Herschel* contours of the Perseus, Taurus, and California clouds are shown in blue (denoted in the top-left panel as Per, Tar, and Cal, respectively). The Per-Tau shell (Bialy et al. 2021) is depicted as a white dot-dashed circle and the Per2 shell is approximated as the green dashed circle. *Top-left panel*: *Hα* observations (Finkbeiner 2003). *Top-right panel*: dust observations from the *Planck* Space Observatory. *Lower-left panel*: HI observations at a velocity of -1.2 km s^{-1} from HI4PI. *Lower-right panel*: composite CO survey of Dame et al. (2001).

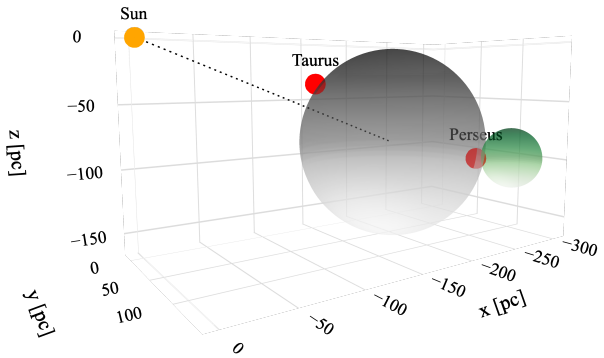


Fig. 7. 3D approximation of the region surrounding the Perseus and Taurus molecular clouds. The approximate locations of the Perseus and Taurus molecular clouds are shown as red circles, and the Per-Tau shell (Bialy et al. 2021) is shown as a gray sphere. The Sun is depicted as a yellow circle and the line-of-sight path connecting the Sun to the center of the Per-Tau shell is shown as a dashed line. The Per2 shell-like structure is approximated as a sphere located behind the Perseus cloud, shown in green. The size of the Taurus and Perseus clouds and the Sun are not depicted to scale.

the Galactic center (8.5 kpc) and orbital velocity (220 km s^{-1}), we find a Galactic rotation velocity (LSR) of approximately -2 km s^{-1} for the Perseus cloud (with the average longitude, l, of 159.5° and the average distance, d, of 294 pc). Although recent studies (e.g., Russeil et al. 2017; Krełowski et al. 2018) have revisited the standard Galactic rotation models of Clemens (1985) and Brand & Blitz (1993), the Clemens (1985) model is sufficient for our purposes.

To estimate the average HI velocity of the cloud, we study the HI spectrum at various points on the cloud. We pick locations for which the HI spectrum shows a single HI peak; namely, it does not exhibit multiple distinguishable peaks, absorption, or significant self-absorption patterns. The HI emission spectrum of these points can be mainly described by a single Gaussian fit. To estimate the average CO velocity, we smoothed the CO data to the same spatial full width at half maximum as the HI data and re-gridded the CO data cube to match the HI cube. With the smoothed and re-gridded CO data, we follow the same approach as explained for HI velocities to obtain the average CO velocity of the cloud. Figure 8 shows an example of these spectra (for HI and CO) for only one sky coordinate in the Perseus cloud. In this figure, the blue line shows the HI line obtained from the HI4PI survey in the left panel, and the observed ^{12}CO $J(1-0)$ line obtained from Dame et al. (2001) in the right panel. The red line shows a Gaussian fit to each spectrum. The x axis shows the LSR velocity and the y axis shows the main-beam brightness temperature.

To find the molecular cloud velocities (CO) in the co-moving frame of the HI gas we use:

$$v_{\mathrm{CO\,-\,HI}} = v_{\mathrm{CO,\,LSR}} - v_{\mathrm{HI,\,LSR}}, \quad (1)$$

where $v_{\mathrm{CO\,-\,HI}}$ is the cloud CO velocity in the co-moving HI frame, $v_{\mathrm{CO,\,LSR}}$ is the CO velocity in the LSR frame, and $v_{\mathrm{HI,\,LSR}}$ is the HI velocity of the region in the LSR frame.

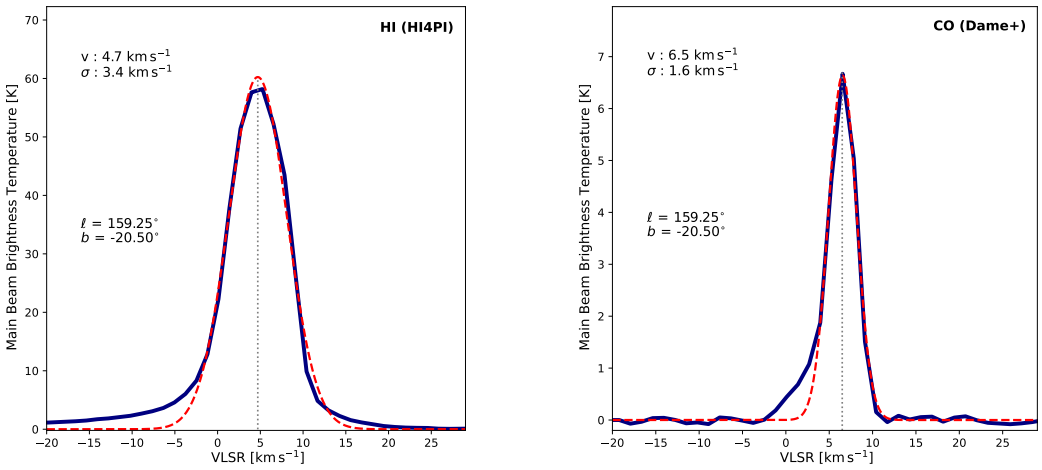


Fig. 8. HI and CO spectra for the Perseus molecular cloud for one coordinate. The blue line shows the HI spectral line obtained from the HI4PI survey in the *left panel* and the observed ^{12}CO $J(1-0)$ line obtained by Dame et al. (2001) in the *right panel*. The red line shows a Gaussian fit to each spectrum. The x axis shows the LSR velocity and the y axis shows the main-beam brightness temperature. In this work, we are interested in the peak emission by CO and HI averaged along the entire cloud.

In this work, we are interested in the peak emission by CO and HI averaged throughout the entire cloud. To estimate the CO velocities in the co-moving HI frame, we adopted three different approaches: (1) averaging CO and HI velocities separately: in this approach, we find both the HI and CO velocities of a number of points across the cloud, determine the average CO and HI velocities, separately, and we use Eq. (1) to find $v_{\rm CO\,-\,HI}$ of the cloud. We find the standard deviation of the averaged velocity centroids ($\sigma_{\rm total}$) to estimate the uncertainty in the mean CO and HI velocities; (2) finding the correlation coefficient: the HI velocities associated with the cloud are more ambiguous than CO due to more line-of-sight confusion and blending effects. To confirm the HI velocity of the cloud, we find the correlation coefficients between HI beam brightness temperature at each velocity slice of the HI4PI data cube and $A_{\rm V}$ values. This approach allows us to find an LSR velocity that corresponds to locations with higher extinction values and is directly linked to the molecular cloud. By studying the HI spectra once separately on the cloud as explained earlier and once using their correlation with $A_{\rm V}$, we ensure that the HI emissions are linked to the cloud of study; (3) obtaining $v_{\rm CO\,-\,HI}$ point by point: we find $v_{\rm CO\,-\,HI}$ for each point (with simple HI and CO spectra) on the cloud separately and determine the average and the standard deviation of all these $v_{\rm CO\,-\,HI}$ values. This approach accounts for any velocity variations and gradients across the cloud.

Figure 9 shows the HI (left panel) and the CO (right panel) velocity locations on the Perseus cloud, which yield an average LSR velocity of $5.3 \pm 1.2\,{\rm km\,s^{-1}}$ and $7.0 \pm 1.6\,{\rm km\,s^{-1}}$, respectively, as explained in the first approach. In this figure, the red circles show LSR velocities away from us and the size of the circles shows their magnitude. The velocities also agree with different studies using HI, ^{12}CO, and ^{13}CO tracers, at similar locations (Imara & Blitz 2011; Arce et al. 2011; Zucker et al. 2018; Remy et al. 2017; Nguyen et al. 2019). We note that the standard deviation values both in CO and HI are largely associated with the velocity gradients along the main axis of the Perseus cloud (which is addressed in the third approach).

To confirm that this HI velocity is associated with the Perseus molecular cloud, as described in the second approach, we found the correlation coefficients between HI beam brightness temperature in each velocity slice and the $A_{\rm V}$ values. We found a peak in the correlation coefficients around an LSR velocity of $5\,{\rm km\,s^{-1}}$, confirming that the average HI velocity that we found in approach 1 is indeed associated with the Perseus cloud. Figure 10 shows the obtained correlation coefficients between HI and $A_{\rm V}$ with a peak around $5\,{\rm km\,s^{-1}}$ (LSR). We note that the HI spectra for the Perseus cloud are relatively easier to analyze compared to other regions in the Galaxy due to its high latitude ($b \sim -20°$). Using these approaches, we found that the average HI velocity associated with the Perseus cloud is smaller than the CO velocity but both have the same direction.

Finally, in the third approach, we compare the CO and HI velocities point by point along the main axis of the Perseus cloud. In this approach, we account for velocity gradients (Ridge et al. 2006; Imara & Blitz 2011) along the cloud and find that the HI emission velocities associated with this cloud tend to be smaller than the CO in absolute value, section by section and point by point. To ensure that our analysis is not impacted by velocity gradients or the uncertainties quoted in the first approach, we find $v_{\rm CO\,-\,HI}$ for a number of points along the cloud (as illustrated in Fig. 11). In this final approach, we make sure that all the considered points have the exact same sky coordinates. The peak CO and HI LSR velocities for these points are shown with red and blue colors in Fig. 11, respectively, and yield an average CO velocity of $1.4 \pm 0.6\,{\rm km\,s^{-1}}$ in the co-moving HI frame (where the 0.6 value is the standard deviation of the offsets in the peak velocities). Therefore, we conclude that for Perseus the average CO velocity in the co-moving HI frame ($v_{\rm CO\,-\,HI}$) is positive (pointing away from us). This implies that, along the line of sight, the CO cloud is moving away from us faster than the HI gas. We can also consider information about the Perseus cloud's surroundings and particularly presence of bubbles in this region.

4.2. Shock-cloud-interaction model

Knowing the $v_{\rm CO\,-\,HI}$ and the GMF directions, we can make a prediction for the $B_{\parallel}$ reversal orientation across the cloud based on the SCI model, and compare it with our reconstructed 3D magnetic field and the $B_{\parallel}$ observations. For example, if the orientation of the GMF (as the initial magnetic fields in the region) and the filament main axis is similar to that of Fig. 4 (where the GMF unit vectors have a perpendicular component to the cloud axis), $v_{\rm CO\,-\,HI}$ toward us would indicate a convex arc-shaped magnetic field morphology, and $v_{\rm CO\,-\,HI}$ away from us would result

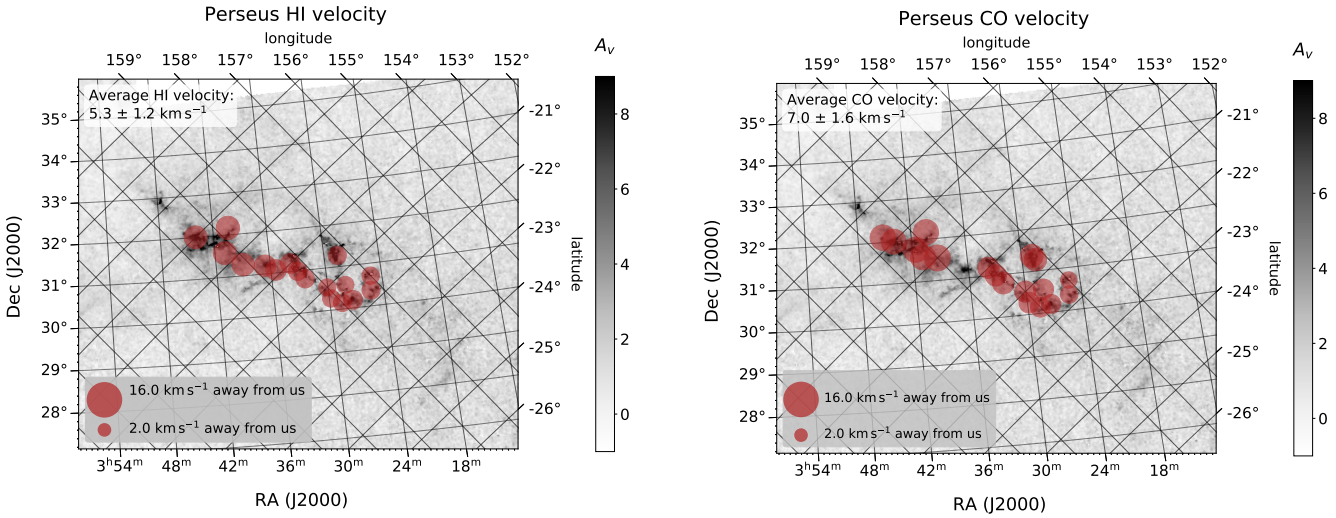


Fig. 9. Perseus molecular cloud HI and CO velocities (LSR) from HI4PI Collaboration (2016) and Dame et al. (2001), respectively. The red circles show velocities pointing away from us. This figure shows our first approach for determining the $v_{\mathrm{CO\,-\,HI}}$ direction, as described in Sect. 4.1. The size of the circles shows the magnitude of the velocities. The background gray-scale image shows the extinction map in A_V magnitude as obtained by Kainulainen et al. (2009). *Left panel*: circles show the HI velocities. *Right panel*: circles show the CO velocities.

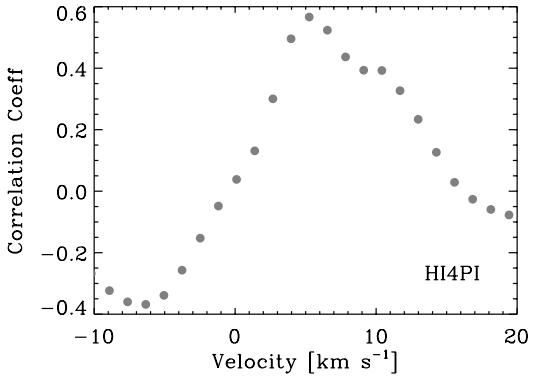


Fig. 10. Correlation coefficients between HI and A_V in the Perseus cloud. To confirm the HI velocities, we find the correlation coefficients between the HI beam brightness temperature and A_V values, at each velocity slice. The y axis shows the correlation coefficient and the x axis shows the LSR velocity. This figure illustrates our second approach for determining the $v_{\mathrm{CO\,-\,HI}}$ direction, as described in Sect. 4.1.

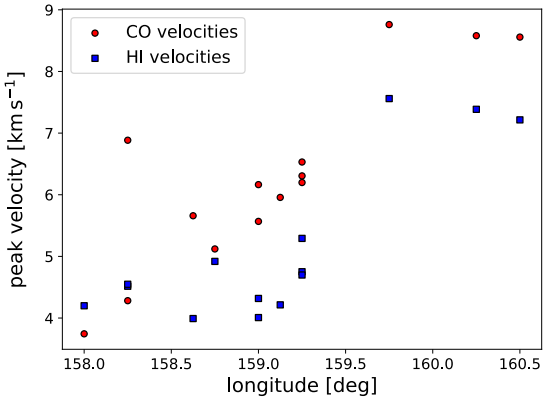


Fig. 11. CO and HI velocities at peak emission in the Perseus cloud. The red circles and blue squares show the velocities at peak emission for CO and HI, respectively. The y axis shows the LSR velocity at peak emission and the x axis shows the longitudes of points. This figure depicts our third approach for determining the $v_{\mathrm{CO\,-\,HI}}$ direction as described in Sect. 4.1.

in a concave arc-shaped magnetic field morphology from our vantage point. Since the GMF vectors are pointing toward $-\hat{\ell}$ direction, we would expect a convex field to result in $B_{\parallel}$ toward us on the southeast side and away from us on the northwest side. We would expect the opposite from a concave field: toward us on the northwest side and away from us on the southeast.

Therefore, the positive CO velocity in the co-moving HI frame indicates that according to the SCI model, the GMF field lines ($-\hat{\ell}$ direction) should be bent and concave from our point of view. This means that the $B_{\parallel}$ observations should result in the fields pointing away from us on the southeast side of the cloud and toward us on the northwest side, which is consistent with the $B_{\parallel}$ observations of Tahani et al. (2018), as shown in Fig. 1, and our reconstructed 3D field morphology, as depicted in Fig. 5. This consistency indicates an even stronger likelihood for the arc-shaped magnetic field morphology.

While the arc-shaped morphology illustrated in Fig. 5 is consistent with the predictions of the SCI model, we note that the morphology might also initially seem consistent with a scenario where the recurrent supernovae associated with the Per-Tau shell have bent and ordered the field lines onto the shell. Examples of this, where the field lines take the shape of the shell and become tangential to the bubble (as the result of being pushed away) have been seen observationally (e.g., Kothes & Brown 2009; Arzoumanian et al. 2021, Tahani et al., in prep.) and theoretically (Kim & Ostriker 2015; Krumholz 2017). If the Perseus cloud's arc-shaped magnetic field morphology is only as the result of tangential field lines to the bubble, then: (1) the $B_{\parallel}$ reversal should be associated with the entire bubble and not specifically associated with the Perseus cloud, and (2) the $B_{\parallel}$ reversal should be relatively weak and not observable. However, the $B_{\parallel}$ observations of Tahani et al. (2018) suggest that the bending is directly associated with the Perseus cloud and does not continue beyond the Perseus cloud.

Moreover, as discussed earlier, CO velocities have a higher magnitude in the direction away from us compared to the

HI velocities. If the cloud has formed by multi-compressions exerted only in the direction of the Per-Tau expansion, the CO velocities should naturally be slower than HI, since, in each expansion, the bubble can push the HI gas further. Therefore, the direct association of the observed $B_{\parallel}$ reversal with the Perseus cloud as well as the positive $v_{\mathrm{CO\,-\,HI}}$ suggest that in addition to the Per-Tau bubble, the cloud has likely been influenced by another structure (pushing the cloud in the opposite direction to the Per-Tau bubble). This interaction has resulted in sharper bending of the magnetic field lines associated with the Perseus cloud and has pushed the HI gas toward us, causing the faster CO velocities in the direction away from us.

To explore this, we investigate the available *Planck* thermal dust emission[6], HI (HI4PI Collaboration 2016), Hα (Finkbeiner 2003), 3D dust (Green et al. 2019), and CO composite maps (Dame et al. 2001), which hint at the presence of a shell-like structure at the far (toward the north) side of the Perseus cloud. This structure has likely interacted with the Perseus cloud and is located on the far edge of the Per-Tau bubble. At the location of this structure, the HI velocities are mostly negative (−5 to 1.2 km s^{-1}) and point toward us, particularly in the co-moving frame of the Perseus cloud. This structure has likely pushed the surrounding HI region of the Perseus cloud toward us, resulting in a sharper bending of the field lines and the observed $v_{\mathrm{CO\,-\,HI}}$.

We refer to this shell-like structure as the Per2 shell or structure, which is consistent with the available 3D dust observations (Green et al. 2019; Zucker et al. 2021, see their Fig. 1). The Per2 structure can be approximated as a circle in the plane of the sky centered at (ℓ = 157°, b = −18°) with a radius of roughly 5°, as shown in Fig. 6. Figure 6 illustrates the Per-Tau and the Per2 shells in white dash-dotted and green dashed circles, respectively. The blue contours show the Perseus, California, and Taurus molecular clouds in the region observed by *Herschel* (Pilbratt et al. 2010). As shown in the top-left panel, the Per2 shell is not identifiable in Hα emission (Finkbeiner 2003), since it is located behind the Per-Tau bubble. The Per2 shell-like structure is visible in *Planck* thermal dust observations, at 353 and 857 GHz (as illustrated in the top right panel of Fig. 6), the CO composite survey of Dame et al. (2001), and the HI4PI HI velocity cube. Additional observations should be carried out in future studies to further confirm the presence of the Per2 bubble and its location.

We suggest that the arc-shaped morphology associated with the Perseus cloud has been shaped by both the Per-Tau and Per2 bubbles: initially, the multi-expansion (due to recurrent supernovae) of the Per-Tau bubble into the region can bend the component of the initial magnetic field that is perpendicular to the propagation direction, resulting in a tangential magnetic field morphology (a mild bending), as shown in the left panel of Fig. 12 (Kim & Ostriker 2015, see their Fig. 16). Subsequently, interaction with the Per2 structure pushes the surroundings of the cloud in the propagation direction of the Per2 shell at the Perseus cloud location (opposite to the Per-Tau bubble propagation direction), resulting in a sharper bending and the arc-shaped magnetic field morphology, as illustrated in the right panel of Fig. 12.

4.3. Other cloud-formation scenarios

We note that simulations by Li & Klein (2019) have found a bent (arc-shaped) magnetic field morphology in their filament formation model using a converging flow scenario (which is similar

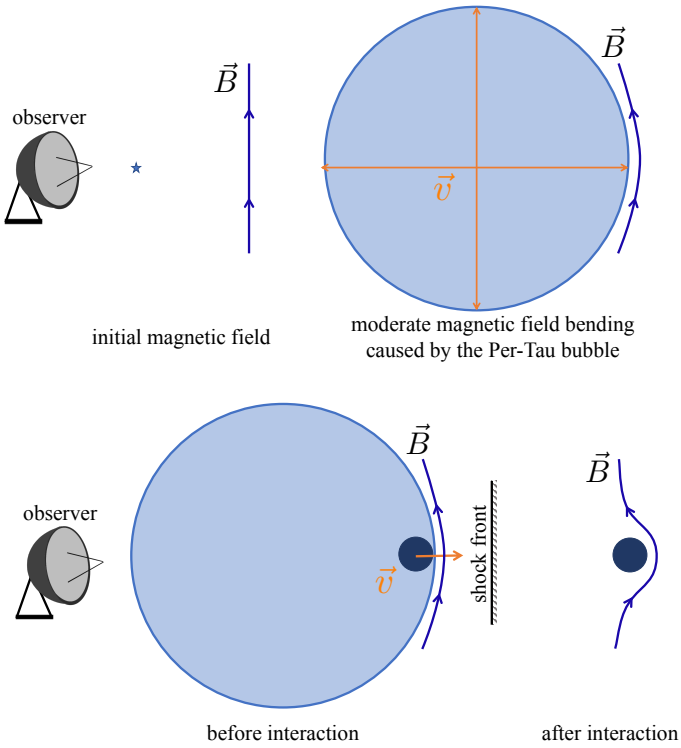


Fig. 12. Formation of the arc-shaped magnetic field morphology in the Perseus cloud. The large light blue circles depict the Per-Tau bubble (created by recurrent supernovae, represented by the star sign). The small dark blue circles depict an end-on view of the Perseus filamentary molecular cloud. *Top panel*: straight ***B*** on the *left* shows the direction of the initial magnetic field before the expansion of the Per-Tau bubble into the region. The curved ***B*** line on the *right* illustrates the large-scale mild bending of the magnetic field morphology after the expansion. *Lower panel*: formation of the arc-shaped magnetic field morphology around the Perseus molecular cloud due to interaction with the Per2 bubble, as described in the SCI model. The blue ***B*** lines show the field lines before and after interaction with the Per2 structure on the *left* and *right*, respectively.

to the SCI model discussed in Sect. 1). In their simulations, Li & Klein (2019) create a ∼4.4 pc-long filament, starting from a homogeneous box, with a sonic Mach number of $\mathcal{M}_s$ = 10, a relatively strong initial magnetic field $\mathcal{M}_{\mathrm{A}}$ = 1.62, and a mean magnetic field strength of 20 μG. Li & Klein (2019) found a long filament forming at the location of converging flows, with bent magnetic field lines. If the initial magnetic field strengths are small, these field lines will be completely perturbed not following any large scale morphology. However, with strong magnetic fields, they find that the cloud retains a memory of the large-scale initial field morphology, even though smaller-scale perturbations in the field lines are detected.

Moreover, a bent magnetic field morphology might potentially be seen in simulations of Körtgen & Banerjee (2015, see their Fig. 10), where they consider a converging flow scenario with 60° angle with respect to the filament (making it a similar case as the SCI model). More cloud formation models (other than the SCI model) could potentially predict arc-shaped magnetic field morphologies. We note that the Perseus cloud with $\ell \sim -20°$ and a distance of ∼300 pc is off the disk and might have a different formation mechanism compared to the clouds located within the disk. Observations of many more molecular clouds at different locations within the Galaxy will allow us to more comprehensively examine the cloud-formation model

[6] *Planck* data release 2: https://wiki.cosmos.esa.int/planck-legacy-archive/index.php/Main_Page

predictions. This study calls for more predictions to be made using various cloud-formation models for a more comprehensive comparison with observations.

5. Discussion: Reconstructed 3D magnetic morphology and its consistency with quantitative analyses

In this section, we further discuss the reconstructed 3D magnetic field morphology, which incorporates 3D Galactic magnetic field models, as well as available $B_{\parallel}$ and $B_{\perp}$ observations. We investigate the influence of variations in the Galactic magnetic field models on the reconstructed field morphology and the consistency of this 3D magnetic field morphology with quantitative data.

5.1. 3D magnetic field morphology

The coherent $B_{\parallel}$ and $B_{\perp}$ observations of the Perseus cloud, as well as the consistency of the $B_{\perp}$ with the GMF vectors projected on the plane of the sky, provide a simple case for reconstructing the 3D magnetic fields in this region. We note that the cloud is located toward the anti-Galactic-center direction and at high latitudes ($\ell \simeq 160°, b \simeq -20°$), resulting in less line-of-sight confusion compared to other clouds in the Galaxy.

The consistency of our 3D magnetic field morphology with the cloud-formation model predictions further supports our reconstructed 3D magnetic morphology. This 3D morphology is also consistent with the effects of bubbles on the Perseus cloud: (a) the Per-Tau bubble has caused a mild and large-scale bending in the field lines; and (b) further interaction with the Perseus cloud's surroundings has pushed the HI gas toward us and caused further field bending, resulting in the $B_{\parallel}$ reversal that is directly associated with the Perseus cloud. The location of the $B_{\parallel}$ observations and their error-weighted strengths indicate that the $B_{\parallel}$ reversal is directly associated with the cloud, caused by the interaction of the field lines with their surroundings.

While we were able to reconstruct the most probable and natural 3D magnetic field morphology in the Perseus cloud and present strong evidence for this 3D field, this study does not rule out other geometries completely. Future high-resolution multi-wavelength observations will allow us to more precisely and accurately determine the clouds' 3D magnetic field morphologies.

5.2. Galactic magnetic field

In Sect. 3.1, we used the JF12 study to estimate the coherent component of the Galactic magnetic field, serving as an approximation for the initial magnetic field of the region in large-scales (before interactions with the surrounding bubble). We found that our modeled GMF is perpendicular to the Perseus cloud and points from the southeast of the cloud to its northwest as shown in Fig. 4. We also found that our modeled GMF vectors follow the same large-scale orientation that the *Planck* $B_{\perp}$ observations obtained in this region, indicating that the cloud retains a memory of the GMF. Since this GMF is approximately perpendicular to the Perseus cloud's axis, even large variations in the coherent GMF models (introduced by different parameters), would not change the overall 3D magnetic field morphology reconstructed in this study or the consistency that we see with the SCI model predictions.

5.3. Age comparisons

Prior to identifying the Per-Tau bubble by Bialy et al. (2021), some studies have identified a large sphere (HI super-shell) associated with the Perseus cloud known as the Per OB2 association, encompassing a longitude range from $\ell = 150°$ to $180°$ and a latitude range of $b = -30°$ to $0°$ (Bally et al. 2008). The age of the Per OB2 sphere was estimated to be from ~6 to 15 Myr (Blaauw 1952, 1964; Borgman & Blaauw 1964; de Zeeuw et al. 1999; Meynet & Maeder 2000; Bally et al. 2008). The Per OB2 association encompasses a number of clusters and young stars. The Perseus cloud, itself, contains two clusters of IC 348 and NGC 1333, with approximate ages of 2 Myr (Luhman et al. 2003) and less than 1 Myr (Lada et al. 1996; Wilking et al. 2004), respectively.

Due to a younger age estimated for the Perseus cloud (1–5 Myr), Bally et al. (2008) suggest that the Per OB2 association has likely triggered the star formation in the Perseus molecular cloud. The Per-Tau shell identified in Bialy et al. (2021) is slightly larger than the Per OB2 sphere, and has a centroid location of ($\ell = 161.1°$, $b = -22.7°$) and a distance of 218 pc, encompassing a longitude range of $\ell = 140°$–$185°$ and latitude range of $b = -40°$ to $0°$. The Per OB2 and Per-Tau bubbles likely represent one bubble. Bialy et al. (2021) estimate the age of the Per-Tau shell to be around 6–22 Myr, and suggest that multiple supernovae compressions from this shell have formed the Perseus molecular cloud.

IC 348, which is located on the eastern side of the cloud and closer to the HI shell identified in previous studies (Shimajiri et al. 2019; Doi et al. 2021), has greater stellar ages compared to the western side of the cloud, and was likely the first region in the Perseus cloud to undergo star formation (Bally et al. 2008). We note that this eastern side of the cloud has larger distances from us compared to its western side (Zucker et al. 2021), which is due to its orientation on the Per-Tau shell identified by Bialy et al. (2021), as shown in their Fig. 2. In addition to different stellar ages across the Perseus cloud, studies suggest that there is a spread in the stellar ages found in IC 348 itself (e.g., Luhman et al. 1998; Muench et al. 2003), which indicates that the region has likely undergone two incidents of star formation (Bally et al. 2008). The scenario illustrated in Fig. 12 can explain the presence of two separate populations of young stars, with different ages, through two epochs of star formation due to interaction with different bubbles in this region: one caused by multiple compressions by the Per-Tau bubble and the other by interaction with the Per2 structure.

5.4. Pressure balance and multi-stage formation of arc-shaped magnetic fields

Bialy et al. (2021) suggest that multiple supernovae have resulted in the Per-Tau shell and the formation of the Perseus molecular cloud. Using estimates of temperature and magnetic field strengths, we can find the gas and magnetic field pressures associated with the Perseus cloud at different evolutionary stages. For this purpose, we use the following equations:

$$P_B = \frac{B^2}{8\pi}[cgs], \qquad P_{\rm gas} = nk_bT, \tag{2}$$

where P_B, B, $P_{\rm gas}$, n, k_B, and T are the magnetic pressure, total strength of magnetic field, gas pressure, particle volume density, Boltzmann constant, and temperature, respectively.

Prior to the formation of the Perseus cloud, we used an estimate of 5 μG for the GMF strength, particle density of 100 cm^{-3}, and an approximate temperature value of a few hundred kelvin (~500 K). We find a magnetic field and gas pressures of 1×10^{-12} bar and 7×10^{-12} bar, respectively. Therefore, magnetic field lines are initially not strong enough to resist the gas pressure and are easily bent and ordered or re-shaped by the bubble expansion (Kim & Ostriker 2015). We note that the mass accumulation along with the bubble expansion result in higher magnetic field strengths on the shell. However, the external gas pressure (during the initial expansions) would still be higher than the magnetic pressure and therefore can further bend the magnetic field lines, resulting in more ordered tangential field lines to the bubble in subsequent expansions.

Simulations by Li & Klein (2019) suggest that in the presence of strong fields $\mathcal{M}_A \simeq 1$, magnetic field lines can coherently bend around a formed filamentary molecular cloud as the result of converging flows, while for $\mathcal{M}_A \simeq 10$, a complete perturbation of magnetic fields should be expected (and no coherent magnetic field morphology). We find the Alfvén mach number using the following equation:

$$\mathcal{M}_A = \frac{\sigma_v}{v_A}, \tag{3}$$

where σ_v is the non-thermal velocity dispersion and v_A is the Alfvén wave group velocity. The Alfvén velocity can be obtained using

$$v_A = \frac{B}{\sqrt{4\pi\rho}}[cgs], \tag{4}$$

where B is the strength of magnetic field and ρ is the volume density. Using a velocity dispersion of 0.6 km s^{-1}, as obtained for the Perseus cloud (Pon et al. 2014), GMF strength of 5 μG, and particle density of 100 cm^{-3}, we estimate the initial $\mathcal{M}_A$ of around 0.5. This $\mathcal{M}_A$ value is approximately two orders of magnitude lower than the $\mathcal{M}_A$ values that could result in fully perturbed field morphologies. Therefore, with $\mathcal{M}_A$ of around 0.5 the field lines should stay coherent (without getting significantly perturbed) and retain a memory of the initial ones. Higher σ_v values (up to 6 km s^{-1}) would still result in $\mathcal{M}_A$ values smaller than what could indicate a completely perturbed field morphology. Moreover, we note that recurrent supernovae at the location of the Perseus cloud have likely enhanced the field strengths associated with this cloud, resulting in lower $\mathcal{M}_A$ numbers.

To calculate the magnetic pressure of the Perseus cloud at its present state, we used the $B_\parallel$ and $B_\perp$ strengths that were previously obtained using Faraday rotation (Tahani et al. 2018), Zeeman measurements (Crutcher 1998; Crutcher et al. 1994; Crutcher & Troland 2000; Troland & Crutcher 2008; Thompson et al. 2019), and Davis Chandrasekhar Fermi method (DCF; Matthews & Wilson 2002; Coudé et al. 2019). The Zeeman and DCF observations mostly fall on the B1 region of the Perseus cloud. The widely cited Zeeman magnetic field strength for B1 is 27 ± 4 μG (Goodman et al. 1989). Using a combination of available Zeeman observations for the $B_\parallel$ strength and the Davis-Chandrasekhar-Fermi (DCF) analysis for the $B_\perp$ strength, Matthews & Wilson (2002) and Coudé et al. (2019) estimated the total strength of the magnetic field in B1 (~100 μG). Moreover, we find the error-weighted average of the $B_\parallel$ strengths obtained by Tahani et al. (2018) to be 136 μG and −90 μG for the magnetic field data that point toward us and away from us, respectively.

Considering these magnetic field strengths, we used an estimate of 100 μG (order of magnitude) for the present-state magnetic field of the Perseus cloud. We find that the magnetic field pressure has a value an order of magnitude higher than the gas pressure, using particle densities of 10^3–10^4 cm^{-3} and temperature of 100 K (Pon et al. 2014) to 12 K, in regions from the cloud surroundings to the dense parts of the filament. We also estimate the $\mathcal{M}_A$ of 0.1 using 0.6 km s^{-1} for the velocity dispersion (Pon et al. 2014). Therefore, the magnetic fields are strong enough to stay coherent and conserve their overall morphology.

The presence of the Per2 shell-like structure can explain these strong magnetic fields (particularly along the line of sight) and their arc-shaped morphology. The enhanced pressure exerted by the Per2 bubble can bend the field lines further, resulting in an arc-shaped field morphology and strong field strengths (~100 μG) directly associated with the Perseus filamentary structure.

In summary, we find that (a) lower magnetic field pressure compared to the gas pressure at initial stages (Per-Tau initial expansions); (b) presence of coherent $B_\perp$ *Planck* observations; (c) presence of coherent $B_\parallel$ morphology; (d) similar orientation of $B_\perp$ and GMF vectors; and (e) the relatively low initial $\mathcal{M}_A$ value strongly suggest that the initial bubble expansions have likely ordered and bent the field lines (instead of completely distorting them). This initial field bending, as shown in the left panel of Fig. 12, is consistent with other observational (e.g., Kothes & Brown 2009) and theoretical (e.g., Kim & Ostriker 2015) evidence; in addition, it is similar to what is seen for HII regions (e.g., Arzoumanian et al. 2021, Tahani et al., in prep.), where the field lines are tangential to bubble edges. This is the first stage of the formation of the arc-shaped magnetic field morphology associated with the Perseus molecular cloud.

Subsequently, the Per2 structure can result in a sharp bending of the field lines directly associated with the Perseus molecular cloud, as illustrated in the right panel of Fig. 12. Compression caused by the interaction with the Per2 structure, and subsequent matter flowing along the field lines and accumulating on the filament, may result in self-gravity dominating the cloud's evolution, triggering a new sequence of star formation. It can also result in further enhancement of $B_\parallel$ strengths associated with the surroundings of the Perseus molecular cloud due to the sharper and more ordered field line bending. Thus, the: (a) spread in the stellar age population; (b) higher CO velocities – compared to HI with their directions pointing away from us; (c) $B_\parallel$ reversal directly and sharply associated with the Perseus filamentary structure; (d) presence of strong magnetic fields (~100 μG); and (e) evidence of a shell-like structure present in the HI, CO, and dust maps suggest that another structure or shell in the region (Per2) has likely interacted with the cloud and bent the field lines around it.

6. Summary and conclusions

We reconstructed the 3D magnetic field morphology associated with the Perseus molecular cloud, using estimates for coherent Galactic magnetic fields (Jansson & Farrar 2012) and recent $B_\parallel$ observations (Tahani et al. 2018). This field morphology is a concave arc shape from our point of view and points from southeast to the northwest of the cloud, in the $-\hat{l}$ direction (toward decreasing Galactic longitude). While different studies (e.g., Clark et al. 2014; González-Casanova & Lazarian 2017; Pattle & Fissel 2019) have provided powerful techniques to probe the plane-of-sky magnetic fields, to our knowledge, this is the

first time that the direction of plane-of-sky magnetic fields (of molecular clouds, scales of ∼10–100 pc) has been mapped.

This field morphology retains a memory of Galactic magnetic fields and is an approximation, which neglects the small-scale magnetic field variations and fluctuations. Therefore, if there are fainter clouds in the foreground of the Perseus cloud (e.g., Ungerechts & Thaddeus 1987), the magnetic fields of these fainter clouds do not interfere with this approximate large-scale arc-shaped magnetic field morphology.

This arc-shaped morphology is consistent with the cloud-formation predictions of the shock-cloud-interaction model (Inutsuka et al. 2015; Inoue et al. 2018). We explored the consistency of the shock-cloud-interaction model with observational data, adding velocity observations and assuming that these velocity observations retain a vestige of the most recent interaction. We studied the GMF direction, as well as the observed HI and CO velocities and made predictions for the $B_{\parallel}$ reversal orientation associated with the Perseus molecular cloud based on the shock-cloud-interaction model. These predictions were consistent with the previous $B_{\parallel}$ observations (Tahani et al. 2018) and our reconstructed 3D magnetic field.

In addition to our finding, some studies (Bally et al. 2008; Doi et al. 2020; Bialy et al. 2021) suggest that the Perseus molecular cloud has formed as the result of bubbles (shock-cloud-interaction) in this region. We suggest that the Per-Tau (Per OB2) bubble has first created a broad-scale mild bending in the field lines. Subsequently, further interaction with the environment has bent the field lines, resulting in an arc-shaped magnetic field morphology directly associated with the Perseus cloud.

While our observations are consistent with the shock-cloud-interaction model, this could be entirely by chance and, therefore, exploring a broad sample of clouds would be necessary. Upcoming rotation catalogs from surveys such as POSSUM (Gaensler et al. 2010) will allow for the determination of $B_{\parallel}$ in many more clouds (Heald et al. 2020). These $B_{\parallel}$ observations can be used to reconstruct the 3D magnetic field morphology of more molecular clouds and to test the observations against predictions from different cloud formation models.

Acknowledgements. We thank the anonymous referee for their insightful comments that helped improve the results and the paper. M.T. is grateful for the helpful discussion with Pak-Shing Li. We have used LaTeX, Python and its associated libraries including astropy (Astropy Collaboration 2013) and plotly (Plotly Technologies Inc. 2015), PyCharm, Jupyter notebook, SAO Image DS9, the Starlink software (Currie et al. 2014), the Hammurabi code, and Adobe Draw for this work. For our line integration convolution plot, we used a Python function originally written by Susan Clark. The Dunlap Institute is funded through an endowment established by the David Dunlap family and the University of Toronto. J.L.W. acknowledges the support of the Natural Sciences and Engineering Research Council of Canada (NSERC) through grant RGPIN-2015-05948, and of the Canada Research Chairs program. Y.D. acknowledges the support of JSPS KAKENHI grant 18H01250. M.H. acknowledges funding from the European Research Council (ERC) under the European Union's Horizon 2020 research and innovation program (grant agreement No 772663).

References

Abe, D., Inoue, T., Inutsuka, S.-i., & Matsumoto, T. 2021, ApJ, 916, 83
André, P., Men'shchikov, A., Bontemps, S., et al. 2010, A&A, 518, L102
André, P., Di Francesco, J., Ward-Thompson, D., et al. 2014, Protostars and Planets VI (Tucson: University of Arizona Press), 27
Arce, H. G., Borkin, M. A., Goodman, A. A., Pineda, J. E., & Beaumont, C. N. 2011, ApJ, 742, 105
Arzoumanian, D., André, P., Didelon, P., et al. 2011, A&A, 529, L6
Arzoumanian, D., Furuya, R. S., Hasegawa, T., et al. 2021, A&A, 647, A78
Astropy Collaboration (Robitaille, T. P., et al.) 2013, A&A, 558, A33
Bachiller, R., & Cernicharo, J. 1984, A&A, 140, 414
Bally, J., Walawender, J., Johnstone, D., Kirk, H., & Goodman, A. 2008, ASP Conf. Ser., 4, 308
Bialy, S., Zucker, C., Goodman, A., et al. 2021, ApJ, 919, L5
Blaauw, A. 1952, Bull. Astron. Inst. Netherlands, 11, 405
Blaauw, A. 1964, ARA&A, 2, 213
Borgman, J., & Blaauw, A. 1964, Bull. Astron. Inst. Netherlands, 17, 358
Bracco, A., Bresnahan, D., Palmeirim, P., et al. 2020, A&A, 644, A5
Brand, J., & Blitz, L. 1993, A&A, 275, 67
Cabral, B., & Leedom, L. C. 1993, Proceedings of the 20th annual conference on Computer graphics and interactive techniques
Chen, C.-Y., King, P. K., Li, Z.-Y., Fissel, L. M., & Mazzei, R. R. 2019, MNRAS, 485, 3499
Clark, S. E., Peek, J. E. G., & Putman, M. E. 2014, ApJ, 789, 82
Clemens, D. P. 1985, ApJ, 295, 422
Coudé, S., Bastien, P., Houde, M., et al. 2019, ApJ, 877, 88
Crutcher, R. M. 1998, Astrophys. Lett. Commun., 37, 113
Crutcher, R. M., & Troland, T. H. 2000, ApJ, 537, L139
Crutcher, R. M., Mouschovias, T. C., Troland, T. H., & Ciolek, G. E. 1994, ApJ, 427, 839
Currie, M. J., Berry, D. S., Jenness, T., et al. 2014, ASP Conf. Ser., 485, 391
Dame, T. M., Hartmann, D., & Thaddeus, P. 2001, ApJ, 547, 792
de Zeeuw, P. T., Hoogerwerf, R., de Bruijne, J. H. J., Brown, A. G. A., & Blaauw, A. 1999, AJ, 117, 354
Doi, Y., Hasegawa, T., Furuya, R. S., et al. 2020, ApJ, 899, 28
Doi, Y., Hasegawa, T., Bastien, P., et al. 2021, ApJ, 914, 122
Finkbeiner, D. P. 2003, ApJS, 146, 407
Fissel, L. M., Ade, P. A. R., Angilè, F. E., et al. 2016, ApJ, 824, 134
Gaensler, B. M., Landecker, T. L., Taylor, A. R., & POSSUM Collaboration 2010, AAS Meeting Abs., 215, 470.13
González-Casanova, D. F., & Lazarian, A. 2017, ApJ, 835, 41
Goodman, A. A., Crutcher, R. M., Heiles, C., Myers, P. C., & Troland, T. H. 1989, ApJ, 338, L61
Green, G. M., Schlafly, E., Zucker, C., Speagle, J. S., & Finkbeiner, D. 2019, ApJ, 887, 93
Haverkorn, M. 2015, Magnetic Fields in Diffuse Media, Magnetic Fields in the Milky Way, eds. A. Lazarian, E. M. de Gouveia Dal Pino, & C. Melioli (Berlin: Springer), 407, 483
Heald, G., Mao, S., Vacca, V., et al. 2020, Galaxies, 8, 53
Heiles, C. 1997, ApJS, 111, 245
Hennebelle, P., & Falgarone, E. 2012, A&ARv, 20, 55
Hennebelle, P., & Inutsuka, S.-i. 2019, Front. Astron. Space Sci., 6, 5
HI4PI Collaboration (Ben Bekhti, N., et al.) 2016, A&A, 594, A116
Houde, M., Dowell, C. D., Hildebrand, R. H., et al. 2004, ApJ, 604, 717
Hu, Y., Lazarian, A., & Yuen, K. H. 2020, ApJ, 897, 123
Imara, N., & Blitz, L. 2011, ApJ, 732, 78
Inoue, T., & Fukui, Y. 2013, ApJ, 774, L31
Inoue, T., Hennebelle, P., Fukui, Y., et al. 2018, PASJ, 70, S53
Inutsuka, S.-i., Inoue, T., Iwasaki, K., & Hosokawa, T. 2015, A&A, 580, A49
Jaffe, T. R. 2019, Galaxies, 7, 52
Jaffe, T. R., Leahy, J. P., Banday, A. J., et al. 2010, MNRAS, 401, 1013
Jansson, R., & Farrar, G. R. 2012, ApJ, 757, 14
Kainulainen, J., Beuther, H., Henning, T., & Plume, R. 2009, A&A, 508, L35
Kerp, J., Winkel, B., Ben Bekhti, N., Flöer, L., & Kalberla, P. M. W. 2011, Astron. Nachr., 332, 637
Kim, C.-G., & Ostriker, E. C. 2015, ApJ, 802, 99
Körtgen, B., & Banerjee, R. 2015, MNRAS, 451, 3340
Kothes, R., & Brown, J.-A. 2009, IAU Symp., 259, 75
Krełowski, J., Galazutdinov, G., & Strobel, A. 2018, PASP, 130, 114302
Krumholz, M. R. 2017, Star Formation (Singapore: World Scientific)
Lada, C. J., Alves, J., & Lada, E. A. 1996, AJ, 111, 1964
Li, H.-b., & Houde, M. 2008, ApJ, 677, 1151
Li, P. S., & Klein, R. I. 2019, MNRAS, 485, 4509
Lombardi, M. 2009, A&A, 493, 735
Luhman, K. L., Rieke, G. H., Lada, C. J., & Lada, E. A. 1998, ApJ, 508, 347
Luhman, K. L., Stauffer, J. R., Muench, A. A., et al. 2003, ApJ, 593, 1093
Matthews, B. C., & Wilson, C. D. 2002, ApJ, 574, 822
McClure-Griffiths, N. M., Pisano, D. J., Calabretta, M. R., et al. 2009, ApJS, 181, 398
McKee, C. F., & Ostriker, E. C. 2007, ARA&A, 45, 565
Meynet, G., & Maeder, A. 2000, A&A, 361, 101
Molinari, S., Swinyard, B., Bally, J., et al. 2010, A&A, 518, L100
Muench, A. A., Lada, E. A., Lada, C. J., et al. 2003, AJ, 125, 2029
Nguyen, H., Dawson, J. R., Lee, M.-Y., et al. 2019, ApJ, 880, 141
Pattle, K., & Fissel, L. 2019, Front. Astron. Space Sci., 6, 15
Pattle, K., Lai, S.-P., Hasegawa, T., et al. 2019, ApJ, 880, 27
Pilbratt, G. L., Riedinger, J. R., Passvogel, T., et al. 2010, A&A, 518, L1
Planck Collaboration Int. XXXII. 2016, A&A, 586, A135
Planck Collaboration Int. XXXV. 2016, A&A, 586, A138

Planck Collaboration Int. XLII. 2016, A&A, 596, A103
Plotly Technologies Inc. 2015, Collaborative data science
Pon, A., Johnstone, D., Kaufman, M. J., Caselli, P., & Plume, R. 2014, MNRAS, 445, 1508
Pon, A., Kaufman, M. J., Johnstone, D., et al. 2016, ApJ, 827, 107
Pudritz, R. E., & Ray, T. P. 2019, Front. Astron. Space Sci., 6, 54
Remy, Q., Grenier, I. A., Marshall, D. J., & Casand jian, J. M. 2017, A&A, 601, A78
Ridge, N. A., Di Francesco, J., Kirk, H., et al. 2006, AJ, 131, 2921
Russeil, D., Zavagno, A., Mège, P., et al. 2017, A&A, 601, L5
Seifried, D., & Walch, S. 2015, MNRAS, 452, 2410
Shimajiri, Y., André, P., Palmeirim, P., et al. 2019, A&A, 623, A16
Soler, J. D. 2019, A&A, 629, A96
Soler, J. D., Bracco, A., & Pon, A. 2018, A&A, 609, L3
Tahani, M., Plume, R., Brown, J. C., & Kainulainen, J. 2018, A&A, 614, A100
Tahani, M., Plume, R., Brown, J. C., Soler, J. D., & Kainulainen, J. 2019, A&A, 632, A68
Taylor, A. R., Stil, J. M., & Sunstrum, C. 2009, ApJ, 702, 1230
Thompson, K. L., Troland, T. H., & Heiles, C. 2019, ApJ, 884, 49
Troland, T. H., & Crutcher, R. M. 2008, ApJ, 680, 457
Ungerechts, H., & Thaddeus, P. 1987, ApJS, 63, 645
Van Eck, C. L., Brown, J. C., Stil, J. M., et al. 2011, ApJ, 728, 97
Waelkens, A., Jaffe, T., Reinecke, M., Kitaura, F. S., & Enßlin, T. A. 2009, A&A, 495, 697
Wilking, B. A., Meyer, M. R., Greene, T. P., Mikhail, A., & Carlson, G. 2004, AJ, 127, 1131
Winkel, B., Kerp, J., Flöer, L., et al. 2016, A&A, 585, A41
Zucker, C., Schlafly, E. F., Speagle, J. S., et al. 2018, ApJ, 869, 83
Zucker, C., Speagle, J. S., Schlafly, E. F., et al. 2019, ApJ, 879, 125
Zucker, C., Speagle, J. S., Schlafly, E. F., et al. 2020, A&A, 633, A51
Zucker, C., Goodman, A., Alves, J., et al. 2021, ApJ, 919, 35